J Solid State Electrochem (2008) 12:245–249
DOI 10.1007/s10008-007-0384-3

ORIGINAL PAPER

X-ray diffraction study on phase transition of orthorhombic LiMnO2 in electrochemical conversions

X. Y. Tu · K. Y. Shu

Received: 25 April 2007 / Revised: 4 June 2007 / Accepted: 15 June 2007 / Published online: 25 July 2007

Abstract Orthorhombic $LiMnO_2$ was synthesized by hydrothermal reaction. Phase transition during electrochemical process has been investigated using the high-resolution X-ray diffraction. Contrary to numerous earlier reports, phase analysis of the orthorhombic $LiMnO_2$ electrode cycled for three times evidences the irreversible structure transition from orthorhombic $LiMnO_2$ (*Pmnm*) to spinel $LiMn_2O_4$ (*Fd3m*) and rock salt $Li_{0.5}Mn_{0.5}O$ (*Fm* $\bar{3}$ *m*). Here, the spinel structure with a cell parameter a=8.241 (1) Å has a large cationic disorder on lithium and manganese sites, i.e., about 9% of the Li positions are occupied by Mn and vice versa. For $Li_{0.5}Mn_{0.5}O$, the cell parameter is a= 4.121 (3) Å, and both Li^+ and Mn^{3+} cations occupy the octahedral 4*a* sites with mole ratio 1:1. The quantity of $Li_{0.5}Mn_{0.5}O$ phase is greatly dependent on cycling rate, namely, the higher the current density is, the larger the quantity of formed-rock salt structure is.

Keywords Orthorhombic LiMnO2 · X-ray diffraction · Phase transition

Introduction

Due to its low cost and nontoxicity, lithium manganese oxides have attracted wide attention as cathode materials for rechargeable lithium-ion secondary batteries [1–3]. Although $LiMn_2O_4$ has been widely studied in the Li–Mn–O phase diagram [4–6], an increasing attention is also being paid to *o*-$LiMnO_2$ (orthorhombic $LiMnO_2$) having a zigzag β-$NaMnO_2$ layered structure (space group *Pmnm*), due to a larger theoretical capacity (285 mA h g^{-1}) of the former [7–12].

In the earlier reports, *o*-$LiMnO_2$ prepared at low temperature (T<450 °C) showed high capacity about 200 mA h g^{-1}, and in situ XRD (X-ray diffraction) study demonstrated that *o*-$LiMnO_2$ converted to a spinel structure after the first cycle [13]. Furthermore, Gummow and Thackeray [14] confirmed the opinion of Reimer et al. that electrochemical cycling of *o*-$LiMnO_2$ prepared at 300 °C resulted in a gradual phase transformation to spinel phase and suggested that the newly formed $LiMn_2O_4$ is significantly more tolerant to repeated lithium insertion and extraction. As mentioned above, subsequent studies had shown that cycling of *o*-$LiMnO_2$ synthesized at high temperature (T>800 °C) induced a progressive phase transformation to spinel structure. In this regard, for the first time, they revealed that the cycle-induced spinel phase consisted of nanodomains confirmed by the observation of high-resolution transmission electron microscopy so that they played a significant role in maintaining a higher capacity in 3 V region [15, 16]. Moreover, by means of in situ XRD experiments, Kim et al. found that a sample with a high number of stacking faults underwent easier phase transformation from orthorhombic structure to spinel one on cycling. This form of *o*-$LiMnO_2$ displayed no capacity fading in the 4 V region but suffered from severe capacity fading in the 3 V region [17]. More recently, in situ synchrotron diffraction showed that *o*-$LiMnO_2$ transformed to a new phase during the first charge process, which was metastable and could easily convert to spinel $LiMn_2O_4$ in the following cycles [18]. The progressive formation of this spinel phase was responsible for the capacity increase in the battery in the initial cycles.

X. Y. Tu (✉) · K. Y. Shu
Department of Materials Science and Engineering,
China Jiliang University,
Hangzhou 310018, People's Republic of China
e-mail: xiaoyantu@163.com

From above reviews, it can be seen that electrochemical cycling of *o*-$LiMnO_2$ compound, prepared at either low temperature or high temperature, often results in phase transformation that has a critical impact on charge and discharge capacity and cycle life. In this work, high-resolution XRD was employed to study phase transition of *o*-$LiMnO_2$ during electrochemical process and more detailed structures were refined by program Jade 6.0.

Experimental

o-$LiMnO_2$ was prepared as follows: 2.0 g Mn_2O_3 (obtained by calcination of Mn_2CO_3 at 700 °C for 3 h in air) was hydrothermally treated with $LiOH{\cdot}H_2O$ aqueous solution (100 ml) at molar ratio of Li/Mn=20:1 in a teflon-lined stainless-steel vessel and autoclaved at 200 °C for 1 h. After cooling to room temperature, the products were repeatedly washed with distilled water until pH value was close to 7.0 and then dried for 0.5 h at 120 °C in air.

The stainless steel model batteries Li/$LiPF_6$ [ethylene carbonate (EC) + dimethyl carbonate (DMC)]/*o*-$LiMnO_2$ were fabricated to elucidate the phase transformation of *o*-$LiMnO_2$ material. The *o*-$LiMnO_2$ electrodes were made by casting a slurry, consisting of 85 wt.% active $LiMnO_2$ powder, 5 wt.% acetylene black, and 10 wt.% PTFE (polytetrafluoroethylene) binder, on Al current collector. The electrode having 10 mg active material with a diameter of 1 cm and thickness of 0.22 mm was then pressed at 18 MPa for 1 min and vacuum-dried at 120 °C for 2 days. The cells were assembled in an argon-filled glove box using a polypropylene (PP) microporous film as a separator, a solution of 1 M $LiPF_6$ in EC/DMC (1:1 ratio in weight) as the electrolyte, and 99.9% metallic Li foils as counter electrodes. The cells were galvanostatically charged and discharged at 0.1 C rate with a voltage window of 2.0–4.5 V at 25 °C.

To investigate the structure changes of *o*-$LiMnO_2$ on cycling, the model batteries were dismantled in an Ar-filled glove box, washed with dimethyl carbonate to remove $LiPF_6$, and dried at 50 °C under vacuum for several hours. After checking the stability in air, the materials were transferred to crystal Si substrate for XRD analysis. Contrary to Al substrate, Si substrate has no peak appearing in the range of 2θ=10–140°, which ensured the accurate statistics on powder. The XRD measurements were performed on a Rigaku D/Max 2500/PC diffractometer with CuK_α radiation operating at 40 kV and 300 mA. For precise determination of the measurements, the powder diffraction patterns were recorded in the range of 2θ=10–80° or 10–140° by step scanning, using 2θ increments of 0.04° and fixed counting time of 4 s/step. The structure refinement and quantitative analyses were performed using the program Jade 6.0.

Results and discussion

As shown in Fig. 1, all the diffraction peaks can be indexed based on the orthorhombic crystal system with a space group *Pmnm*. The calculated cell parameters of the pure *o*-$LiMnO_2$ are α=4.557 (3) Å, b=5.756 (2) Å, and c=2.807 (2) Å, which are well coincident with the JCPDS card (35-0749) [19].

Figure 2 depicts the charge and discharge potential profiles of *o*-$LiMnO_2$ electrode at 0.1 C rate between 2 and 4.5 V at 25 °C. The first charge potential profile is dominated by a voltage plateau around 3.5 V, which is

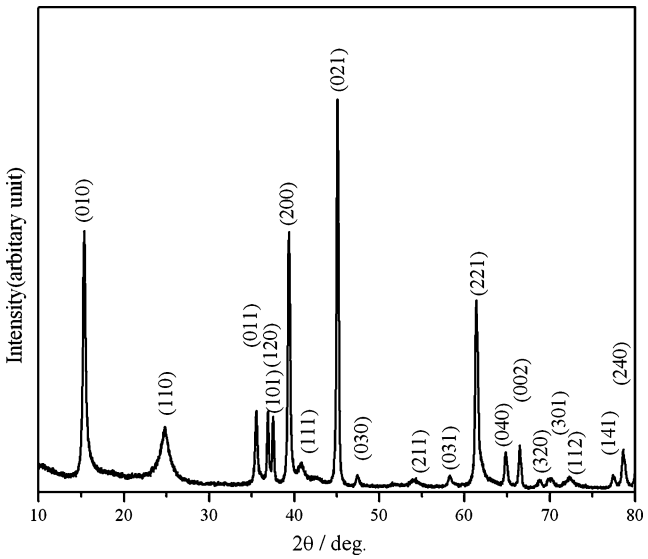

Fig. 1 XRD pattern of *o*-$LiMnO_2$ powder

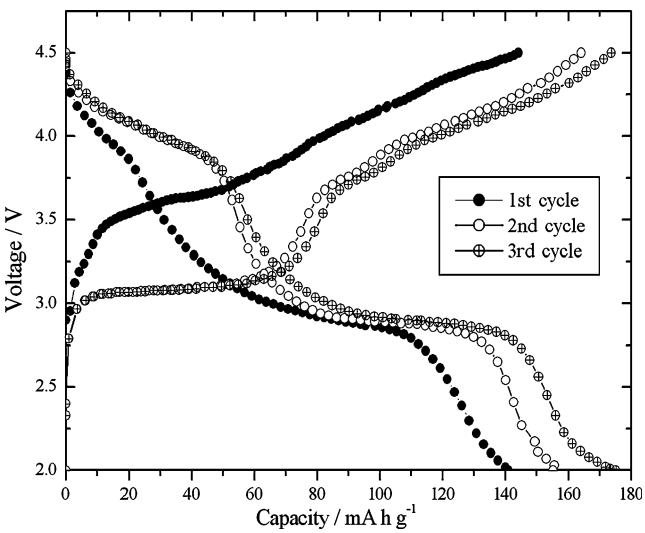

Fig. 2 Charge and discharge potential profiles of the *o*-$LiMnO_2$ electrode for initial three cycles

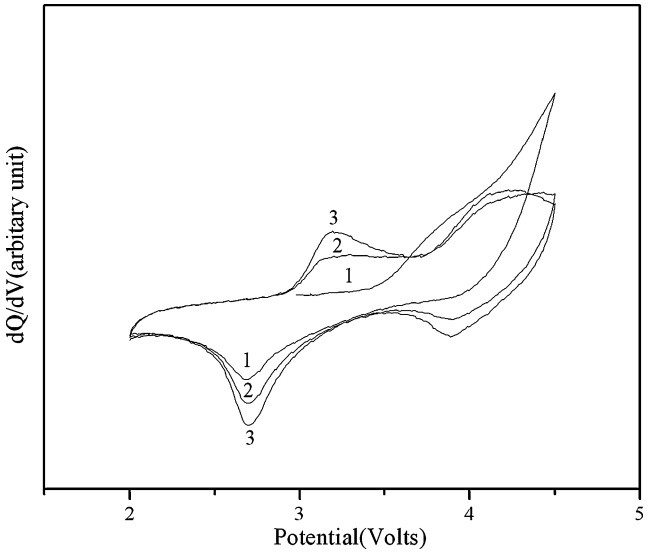

Fig. 3 Differential capacity (dQ/dV) vs potential curves of the *o*-$LiMnO_2$ electrode for initial three cycles

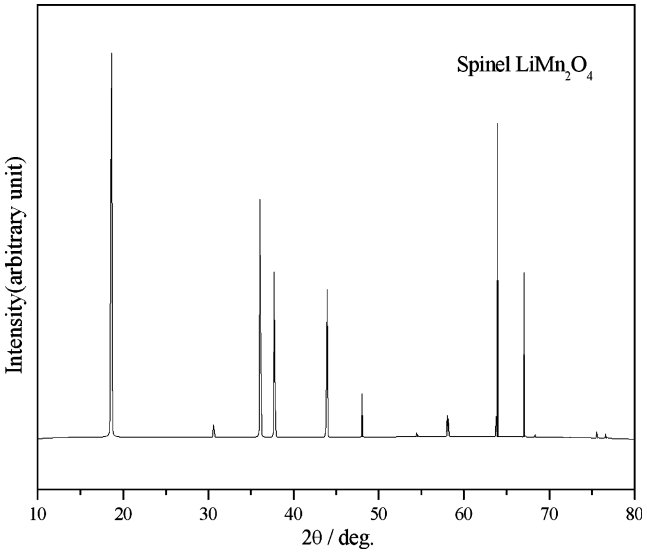

Fig. 5 XRD pattern of spinel $LiMn_2O_4$ calculated by the cubic spinel model

completely different from that of the subsequent first discharge. Obvious discharge voltage plateaus around 4 and 3 V appear from the second cycle. This means that some irreversible reactions may occur during the initial cycles [20]. Differential capacity (dQ/dV) plots are also displayed in Fig. 3. It can be seen from the figure that two apparent redox peaks appear from the second cycle, especially in third cycle, which is in good accordance with the potential profile changes in Fig. 2. The enhancement of the incremental redox peaks is proportional to the amount of active cathode material progressively formed in the initial cycles providing the charge and discharge capacities of the Li | *o*-$LiMnO_2$ battery.

To further investigate the structural evolution, the *o*-$LiMnO_2$ electrodes of 1-, 2-, 3-, 10-, and 20-cycled discharged to 2 V at 0.1 C rate were analyzed by XRD. As shown in Fig. 4, by the end of the first discharge process, the intensities of the peaks of $LiMnO_2$ decrease, and in the meanwhile, some new peaks appear. After three cycles, the *o*-$LiMnO_2$ could not be found from the diffraction patterns, indicating that the cathode material has completely transformed to new phases, which is consistent with the changes of the voltage plateaus (Fig. 2) and redox peaks (Fig. 3). It can be observed that the diffraction peaks of the new phases become broader than that of the pristine *o*-$LiMnO_2$. This suggests that the formation of defects (e.g., microstrain and stacking faults)

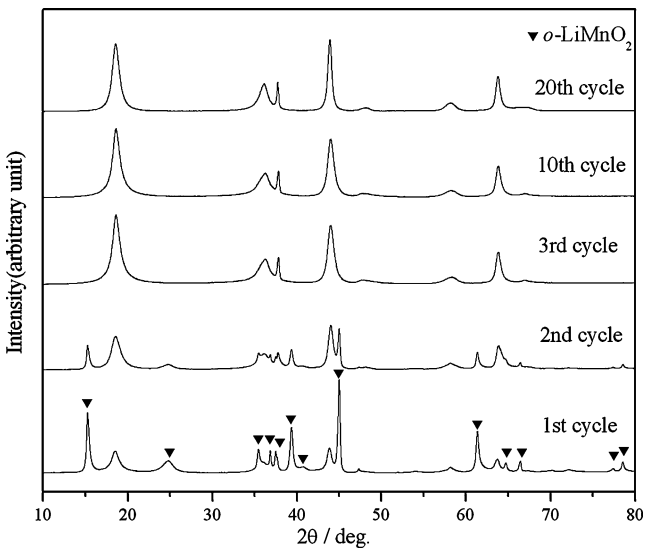

Fig. 4 XRD pattern evolution of the *o*-$LiMnO_2$ electrodes after different cycles

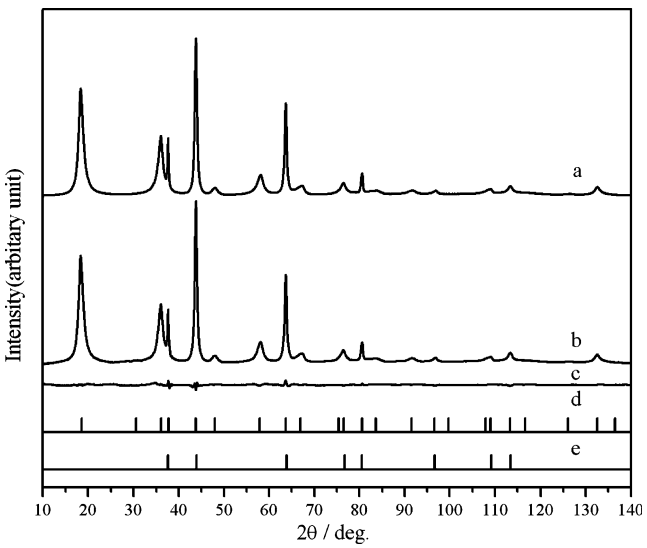

Fig. 6 The Rietveld refinement of the *o*-$LiMnO_2$ electrode cycled for three times discharged to 2 V at 0.1 C rate. The *curves* are calculated XRD pattern, observed XRD pattern, and the difference between them from *a* to *c*. The *reflection marks* belong to the phases of spinel $LiMn_2O_4$ (*d*) and rock salt $Li_{0.5}Mn_{0.5}O$ (*e*). The weighted patter factor R_{wp}=9.57, the bragg factor R_b=8.23, and the goodness of fit S=1.32

Table 1 Structure parameters obtained from Rietveld refinement of the *o*-$LiMnO_2$ electrode cycled for three times discharged to 2 V at 0.1 C rate

Phase	Space group	Cell parameter α (Å)	Atom site		Atom position			Occupancy	Phase ratio (wt.%)
					x	y	*z*		
$LiMn_2O_4$	*Fd3m*	8.241 (1)	Li_1	8a	1/8	1/8	1/8	0.9114	88.9
			Mn_1	8a	1/8	1/8	1/8	0.0886	
			Li_2	16d	1/2	1/2	1/2	0.0851	
			Mn_2	16d	1/2	1/2	1/2	0.9149	
			O	32e	0.2765(4)	0.2765(1)	0.2765(5)	0.9965	
$Li_{0.5}Mn_{0.5}O$	*Fm* $\bar{3}$ *m*	4.121 (3)	Li	4a	0	0	0	0.4995	11.1
			Mn	4a	0	0	0	0.5005	
			O	4b	1/2	1/2	1/2	1.002	

in the material lattice or that the crystal particles have been cracked into some smaller ones during the electrochemical process, which may improve the material electrochemical properties [21]. After a careful comparison, one may notice that the newly appeared peak positions are very similar to those obtained from spinel $LiMn_2O_4$ in Fig. 5 [22, 23]. However, the relative strength ratio of the peaks is not completely consistent with $LiMn_2O_4$, which may indicate that another new phase exists.

It is necessary to clarify the structural changes as it is closely related to the electrochemical properties. At present we have concentrated on the challenge to investigate how phases change on cycling by XRD. Rietveld refinement of the *o*-$LiMnO_2$ electrode cycled for three times discharged to 2 V at 0.1 C rate was performed using the cubic spinel and rock salt structural models [23]. The phase-fitting patterns of the electrode and the refined structural parameters are shown in Fig. 6 and Table 1, respectively. Based on these observations it can be concluded that after three cycles, the irreversibly structure transition from *o*-$LiMnO_2$ (*Pmnm*) to spinel $LiMn_2O_4$ (*Fd3m*) and rock salt $Li_{0.5}Mn_{0.5}O$ (*Fm* $\bar{3}$ *m*) with 88.9 and 11.1 wt.%, respectively, have taken place. Up to now, it is generally accepted that the *o*-$LiMnO_2$ will convert to spinel $LiMn_2O_4$ on cycling [10, 22]. Here, in more details, the $LiMn_2O_4$ structure with a cell parameter α=8.241 (1) Å has a large cationic disorder on lithium and manganese sites, i.e., about 9% of the Li positions are occupied by Mn and vice versa, which may improve its electrochemical behavior compared with that of the ordered phase [21]. On the other hand, this is the first time to report $Li_{0.5}Mn_{0.5}O$ phase with space group *Fm* $\bar{3}$ *m*. The cell parameter of $Li_{0.5}Mn_{0.5}O$ is α= 4.121 (3) Å, about half that of spinel $LiMn_2O_4$. And both Li^+ and Mn^{3+} cations occupy the octahedral 4*a* sites with mole ratio 1:1. There is at least one factor that may affect the apparent inconsistency of the structural data presented in this paper. Namely, the resolution of the X-ray instrument used is not sufficient and, because of the partial peaks overlapping, the spinel structure and rock salt one could be indistinguishable. In the previous study, Chiang et al. [16] had hypothesized that the structural transformation from orthorhombic to cubic spinel occurred via an intermediate disordered rock salt structure with a space group of *Fm* $\bar{3}$ *m*. Different from their opinion, the rock salt structure demonstrated here is stable with the coexistence of spinel $LiMn_2O_4$ upon further cycling, as there are no obvious changes in XRD patterns of the *o*-$LiMnO_2$ electrodes after 10 or 20 cycles in Fig. 4. Other researchers proposed that the transformation from *o*-$LiMnO_2$ to spinel needs the migration not only of all the lithium ions but also of half of the manganese ions [24]. According to their points, we consider that, in electrochemical process, there is not enough time for the migration of all lithium and manganese ions to form spinel structure. Therefore, at the end of discharge stage, part of rock salt phase still exists. In addition, the quantity of $Li_{0.5}Mn_{0.5}O$ phase formed with cycling is greatly dependent on cycling rate, as illustrated in

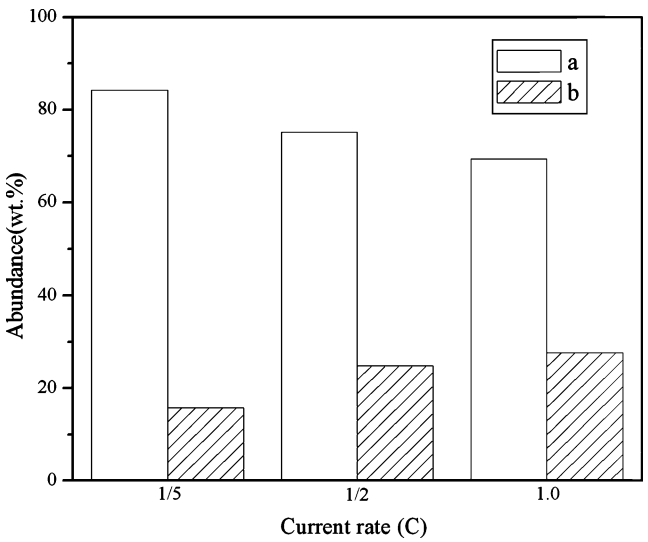

Fig. 7 The phase abundance of spinel $LiMn_2O_4$ (*a*) and rock salt $Li_{0.5}Mn_{0.5}O$ (*b*) at different current rates

Fig. 7. The higher the current density is, the larger the abundance of formed-rock salt structure is. It is probably that, applying higher current density, the faster de-/intercalation process of lithium ions would lead to a higher local lithium concentration, thus hindering structural reordering of rock salt phase to spinel one.

Conclusions

The XRD results presented above show clearly that the phase transition occurred in the initial cycles. Rietveld refinement of the *o*-$LiMnO_2$ electrode cycled for three times reveals the irreversible structure transition from *o*-$LiMnO_2$ (*Pmnm*) to spinel $LiMn_2O_4$ (*Fd3m*) and other new phase (rock salt $Li_{0.5}Mn_{0.5}O$ with space group $Fm\ \overline{3}\ m$). Both of them coexist upon further cycling. In addition, the quantity of $Li_{0.5}Mn_{0.5}O$ phase is greatly relative to the current density. The higher the current density is, the larger the quantity of formed-rock salt structure is. Further studies aiming at investigating the electrochemical behavior of rock salt phase are currently in progress.

Acknowledgments The authors would like to appreciate the financial support of Natural Science Foundation of China Jiliang University (no. x20536).

References

1. Hatzikraniotis E, Kokkou S (1998) J Power Sources 72:22
2. Hwang BJ, Santhanam R, Hu SG (2002) J Power Sources 108:250
3. Kim J, Fulmer P (1999) Mater Res Bull 134:571
4. Xia YY, Takeshige H (1995) J Power Sources 56:61
5. Sun YK, Jeon YS (1999) Electrochem Commun 1:597
6. Park SH, Park KS, Moon SS, Sun YK, Nahm KS (2001) J Power Sources 92:244
7. Lee YJ, Grey CP (2000) Chem Mater 12:3871
8. Komaba S, Myung ST (2002) Solid State Ionics 152–153:311
9. Myung ST, Komada S, Kumagai N (2002) Solid State Ionics 150:199
10. Lu CH, Wang HC (2004) J Eur Ceram Soc 24:717
11. Kim TJ, Dongyeon S, Jaephil C, Byungwoo P (2006) J Power Sources 154:268
12. Kellerman DG, Medvedeva JE, Gorshkov VS, Kurbakow AI (2007) Solid State Sci 9:196
13. Reimers JN, Fuller EW, Rossen E, Dahn JR (1993) J Electrochem Soc 140:3396
14. Gummow RJ, Thackeray MM (1994) J Electrochem Soc 141:1178
15. Wang H, Jang YI, Chiang YM (1999) Electrochem Solid-State Lett 2:490
16. Chiang YM, Wang HF, Jang Y (2001) Chem Mater 13:53
17. Kim JM, Chung HT (2003) J Power Sources 115:125
18. Wei YJ, Ehrenberg H, Bramnik NN, Nikolowski K, Baehtz C, Fuess H (2007) Solid State Ionics 178:253
19. Wang GX, Yao P (1999) J Appl Electrochem 29:1423
20. Ohzuku T, Kitagawa M (1990) J Electrochem Soc 137:769
21. Croguennec L, Denniard P, Brec R (1997) J Electrochem Soc 144:3323
22. Jaephil C, Michael MT (1999) J Electrochem Soc 146:3577
23. Michael B (1997) ICSD/RETRIEVE 2.01
24. Tang WP, Hirofumi K, Kenta O (1999) J Solid State Chem 142:19